

Article

Not peer-reviewed version

Wind Effects on Re-entrant Wing Faces of Plus Plan Shape Building

Arun Kumar , [Rahul Kumar Meena](#) , [Ritu Raj](#) , [Mohammad Iqbal Khan](#) ^{*} , [Jamal M. Khatib](#)

Posted Date: 9 November 2023

doi: 10.20944/preprints202311.0652.v1

Keywords: “+” shape model; re-entrant corners; pressure coefficient; k-e model; tall building



Preprints.org is a free multidiscipline platform providing preprint service that is dedicated to making early versions of research outputs permanently available and citable. Preprints posted at Preprints.org appear in Web of Science, Crossref, Google Scholar, Scilit, Europe PMC.

Copyright: This is an open access article distributed under the Creative Commons Attribution License which permits unrestricted use, distribution, and reproduction in any medium, provided the original work is properly cited.

Article

Wind Effects on Re-Entrant Wing Faces of Plus Plan Shape Building

Arun Kumar ¹, Rahul Kumar Meena ², Ritu Raj ¹, Mohammad Iqbal Khan ^{3,*} and Jamal M. Khatib ⁴

¹ Department of Civil Engineering, DTU, India; arunkumar.dtu@gmail.com (A.K.), rituraj@dtu.ac.in (R.R.)

² Department of Civil Engineering, Punjab Engineering College, Chandigarh, India; rahul.08dtu@gmail.com (R.K.M.)

³ Department of Civil Engineering, College of Engineering, King Saud University, P.O. Box 800, Riyadh 11421, Saudi Arabia;

⁴ Faculty of Science and Engineering, University of Wolverhampton, Wolverhampton WV1 1LY, UK; j.m.khatib@wlv.ac.uk (J.M.K.)

* Correspondence: miqbal@ksu.edu.sa (M.I.K.)

Abstract: The wind flow patterns and pressure distribution around a plus-shaped building are significantly influenced by the dimensions of its re-entrant corners and the overall building height. The present study aims to find the wind effects and study of the pressure distribution with different flow patterns. Plan area of the building is around 300 square meter while the height of the building is 50 meters by keeping the equal length of the re-entrant corners. The research is performed using ANSYS CFX academic version and the results are depicted in various forms such as pressure coefficient (C_{pe}), stream lines in both vertical as well as in specific surface and pressure contours. The analysis is carried out by varying the wind incident angles, from 0° to 90° at the interval of 15°. The building dimension are scale down to perform the test on length scale of 1:100. Since the considered building model exhibits symmetry along both the axes, present study mostly emphasis on examining re-entrant corners located in the building. This method yields valuable information about how air circulates and how pressure is distributed across a broad spectrum of wind angles. This study provides valuable insights into flow circulation and pressure distribution for a wide range of wind angles.

Keywords: “+” shape model; re-entrant corners; pressure coefficient; k-e model; tall building

1. Introduction

The increasing utilization of diverse construction materials and innovative designs in the field of high-rise building construction underscores the necessity for precise insights into wind dynamics and pressure distribution across building facades. The knowledge is essential for achieving a harmonious balance between the functional and structural aspects of building design. While extensive research has been conducted on conventionally structured building models, serving as the foundation for the development of international wind design codes in various countries. Codal values remains a noticeable scarcity of research focused on buildings with irregular plan shapes. The research gap calls for a deeper understanding of the unique challenges posed by irregular building designs and underscores the importance of conducting comprehensive investigations in this domain. A general estimation of magnitude of wind pressure on faces of any bluff body is taken as mean pressure coefficient (C_{pe}). It is a dimensionless measure which largely depends upon the shape and size of the bluff body, and surrounding topographical characteristics. External mean pressure coefficient (C_{pe}) is almost independent of the velocity of flow. The oblique wind also creates different wind flow pattern around the body, and results in varying velocity pressure on the surfaces.

Investigating wind effects through a combined approach of numerical simulations and real-world experiments is a critical endeavour in understanding and mitigating the impact of wind on

various high-rise structures. This interdisciplinary approach enables researchers and engineers to gain comprehensive insights into the behaviour of wind, contributing to more effective design and safety measures. The wind effects on a high-rise building model may be explored using experimental (wind tunnel method) as well as using numerical simulation. Few researchers studied pressure pattern on a square shape building model [1–3] The contour isobars of mean wind pressure on different faces of the model. It was demonstrated that upwind side of the model is exposed to positive pressure but on side faces, top and backward faces, negative pressure do exist. Subsequently, pressure distribution and wind load studies on varying size and height of regular tall buildings such as square, rectangular, circular etc. were carried out by different researchers. Guidelines for design of structures against wind loads have been made after analysing wide range of data from the studies and international standards [4–9] (field measurements and experimental studies) in the form of codes/standards. But due to scarcity of land in urban and metropolitan cities and evolution of new construction materials and technologies, height of the buildings has to be maximized along with usage of irregular shapes as building cross section, to fit in the available topography of land. Wind tunnel studies are conducted to investigate the wind generated effects on high rise structures, which is time consuming and cumbersome. Using the latest technology and development in the computational resources now a days numerical simulations are gaining importance. It provides faster and economical solution within the comfort of office. Full scale measurements can also be done in numerical simulations. Behavior of irregular shape buildings under wind load have been studied by many researchers on wind tunnel and/or numerically. For example, wind pressure pattern along the perimeter of L and U shape buildings in plan of similar height were studied on wind tunnel and numerically [10] Similarly, along and across wind effects as well as interference effects on a model of tall rectangular building were studied by [11] by using wind tunnel tests and Computational Fluid Dynamics (CFD). It is observed from the study is that the percentage difference between the results from wind tunnel test and CFD to be between 20 % to 25 %. Field measurement results of two super tall buildings were compared with wind tunnel data for two terrain characteristics – open country and urban terrain [12]. The predicted design load (p_d) value for clad buildings is modified by wind directionality factor (K_d) and area averaging factor (K_a) [4]. Various research works is in the field of wind engineering on irregular shapes of buildings. Aerodynamic forces and wind pressure on various unconventional plan shaped tall buildings were presented by [13,14]. The wind directionality and side ratio of a rectangular building modify suction pressure on side faces and lee face. Pressure envelope around the faces of a regular E plan shape building model for various wind directions was studied by [15]. Fluctuating forces and pressure due to wind on a super tall building model for isolated and surrounded conditions for different wind directions were studied [16]. The wind flow parameters around N cross-section of tall building [17]. Surface pressure on faces of a C-shaped building model with different aspect ratio was investigated [18] on ANSYS (Fluent) using $k - \epsilon$ turbulent model for different wind incidence angles and the results were compared with wind tunnel results. Interference effect on a rectangular building due to another building placed to form an L-shape in plan were studied through modelling in STAAD Pro with varying height of the interfering building by [19]. Effect of side ratios on wind imparted load on a Y shape tall building was studied [2,20,21] using numerical simulations. A comparison of results obtained from $k - \epsilon$ and SST turbulence models and experimental data were made. The results from obtained from $k - \epsilon$ turbulence model was similar to wind tunnel experimental results. Although, Plus-plan shape is a very common shape, experiments on such plan shape buildings have generally been conducted for normal wind directions only. [22] investigated wind effects on a plus shape building model with varying re-entrant wing lengths and compared the results with a square model of similar plan area Both, the cross-sectional shapes and wind directions, were found to influence the base shear, base moments, and twisting moment acting on the model. [23] reviewed the results from on a tall building with a plus shape for 0° and 45° wind angles experimentally and numerically, both. It was observed that the variations in pressure coefficients between the wind tunnel test and the numerical approach were within the acceptable range.

In the current research study, a unique and innovative investigation by focusing on the surface pressure distribution of a plus-shaped building model is made the building exhibits distinctive characteristics, with a cross-sectional area of 300 square meters and a height of 50 meters. The main focus of the study lies on the wind generated effects on re-entrant corner of tall building. The numerical simulation is performed using k-epsilon turbulence model, the wind velocity is applied as power low and for the building model the length scale ratio is selected based on the guideline available in various international standards.In this research the coefficient of pressure (C_{pe}), Stream lines in the vertical as well as on the specific surface of re-entrant corners, pressure contours and pressure distribution for various wind incidence angle is presented in different graphical forms.

2. Verification and Validation

Before going for simulation of any irregular shape building model it is necessary to validate the approach with a standard shape model, data of which is available in the texts or codes for comparison. A rectangular cross-sectional model of similar height and cross-sectional area (Figure 2) was simulated under the similar conditions. Comparison of Pressure coefficient of the rectangular model were found to be under acceptable limit when compared with those provided in international codes (Table 1).

Table 1. Comparison of Area Average C_{pe} on Faces of Rectangular Model.

As per	Wind Angle	C_{pe} Face A	C_{pe} Face B	C_{pe} Face C	C_{pe} Face D
ANSYS (CFX)	0°	+ 0.68	- 0.27	- 0.60	- 0.60
	90°	-0.60	-0.60	0.70	-0.28
IS: 875 (Part 3): 2015	0°	+ 0.8	- 0.25	- 0.8	- 0.8
	90°	-0.8	-0.8	0.8	-0.25
ASCE/SEI 7-16	0°	+ 0.8	- 0.5	- 0.7	- 0.7
	90°	-0.7	-0.7	0.8	-0.5
AS/NZS- 1170.2 (2002)	0°	+ 0.8	- 0.5	- 0.65	- 0.65
	90°	-0.65	-0.65	0.8	-0.5
	0°	0.8	-0.55	-0.8	-0.8
EN: 1991-1-4	90°	-0.8	-08	0.8	-0.55

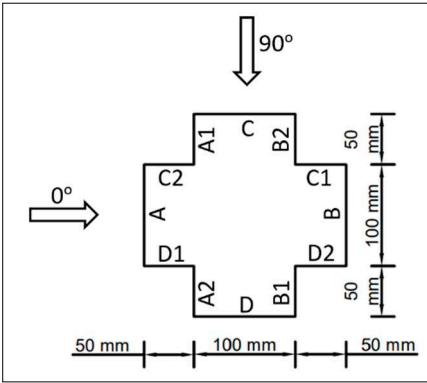


Figure 1. Plus Shape Model.

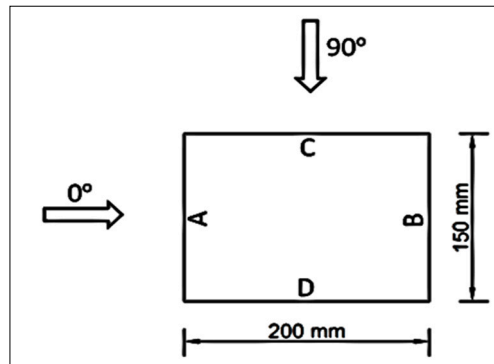


Figure 2. Rectangular Model.

3. Numerical Analysis

Navier-Stokes Equations of fluid flow known as Continuity and Momentum equations are the fundamental equations for defining any fluid flow. Various numerical models have been developed in the form of differential equations on the basis of Navier-Stokes Equations to study the turbulent flow circulation around any bluff body. These differential equations are solved at finite grid locations during simulation. The differential equations contain many unknowns and immeasurable quantities having negligible magnitude. Depending upon the expected flow behavior, assumptions have been made to neglect these negligible quantities. One of the most commonly used models for numerical analysis is the standard $k - \epsilon$ ($k - \epsilon$) turbulence model for bluff body wind simulation. In this model, it is easy to provide initial and/or boundary conditions. However, for complex flows with a high-pressure gradient separation and considerable streamline curvature, it does not perform well. In this model fluid turbulence is defined by two transport equations. The first is 'Turbulent Kinetic Energy (k)' and the second is 'Dissipation of Turbulent Kinetic Energy (ϵ)'. For steady state wind flow condition, a time averaged fluid velocity in the continuity and momentum equations of Navier-Stokes has been assumed. These equations are termed as Reynold's Averaged Navier-Stokes (RANS) equations. The RANS equations and the additional transport equations are defined in ANSYS (CFX) solver theory guide 2012.1 (2009) at page 57 [24].

4. Mean Velocity Characteristics

Vertical profile of wind in nature increases exponentially within the atmospheric boundary layer (ABL) due to friction from surface vegetation, manmade structures on the earth's surface and earth's rotation. Hence, wind load on tall buildings also increases exponentially along height. It is difficult to exactly mimic the vertical wind profile for experimental studies. However, some empirical formulae are available to reproduce the vertical wind profile within the ABL. One of the most used among them is the power law presented below.

Power Law:

$$u = u_{Ref} \left(\frac{Z}{Z_{Ref}} \right)^\alpha \quad (1)$$

In the above equation

u_{Ref} = Time averaged wind speed in m/s

Z_{Ref} = Height at which the time averaged wind speed is taken.

u = Velocity given by the equation at height Z above ground.

α = Terrain roughness index.

Power Law does not provide correct natural wind velocity up to 10 m from surface of earth. But it is simple in its use and suitable for tall structures.

5. Model and Computational Domain

Computational domain is a virtual wind tunnel. Size of the domain is kept large enough so that the blockage of wind flow remains within 3 % due to presence of model. The model, for simulation on isolated condition, is placed inside the domain as shown in Figure 3. The distance of domain boundaries from the outer surface of the model in each direction was adopted as recommended by COST group [25] to ensure appropriate flow conditions around the model envelope. For steady state modelling on tall building recommendation for size of domain by [26] is similar as those in COST group in the matter.

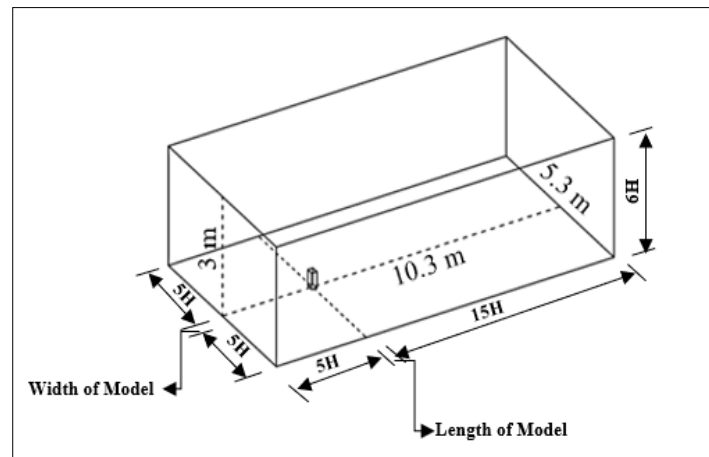


Figure 3. Computational Domain.

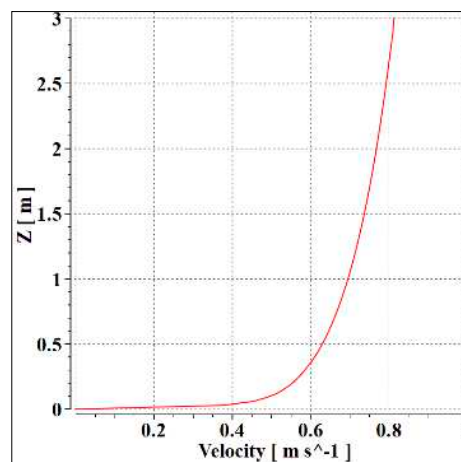


Figure 4. Velocity Profile.

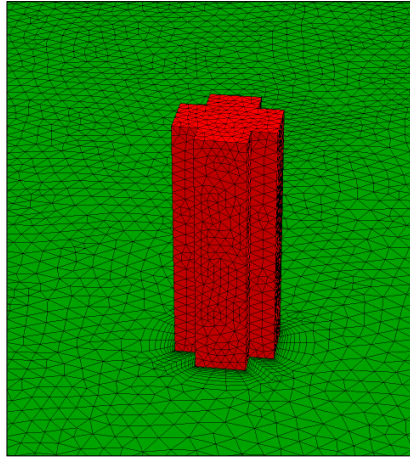


Figure 5. Meshing.

6. Grid Discretization

Simulation result depends upon the grid element sizes of the domain volume and the model. The pressure around the model envelope is mapped with acceptable accuracy when the flow parameters at expected location of high gradient velocity is reproduced correctly. Fine meshing elements are therefore required on the faces. During the simulation of rectangular model, the grid resolution of the domain was set to $1/5^{\text{th}}$ of the building scale with global automatic meshing option, The element size on the domain ground surface was modified using local setting and was taken as $1/2$ the size of the domain volume elements. Grid size on the building surface was made further finer from the local face sizing option to $1/4$ of the global mesh size. Smooth inflation for the model surface elements was provided for mapping the pressure perpendicularly on the surface of the model faces. Maximum skewness of the elements was ensured to be less than 0.9 and the minimum orthogonal quality not less than 0.6 for good results. It was ensured that large variation in the prediction of results does not occur due to change in element size and the predicted value of coefficient of pressure was kept within 20 % to 25 % of the values given in IS Code 875 (Part 3): 2015. Similar meshing was adopted for simulation of plus shape model.

7. Boundary Conditions

Homogeneous steady state wind flow under atmospheric boundary layer for open terrain with well scattered surface obstructions of height 1.5 to 10 m [as per IS: 875 (Part 3): 2015] at the inlet was provided using the terrain roughness index as 0.143. Gustiness effect has been given by providing turbulence intensity of 5 %. Velocity attained at the roof height of the model was found to be 0.63 m/s. This velocity is sufficient to achieve the critical Re for turbulent flow around sharp-edged models like the present one. The velocity profile is shown in Figure 4. Free slip wall condition was provided on the domain side walls and top wall. The roof surface of the model was also provided with free slip wall condition. By providing this condition, it was ensured that flow parallel to the walls is free from frictional forces and is computable during the simulation. No slip wall condition was provided on the model surfaces and the ground of domain to ensure that velocity at the surface is zero for making of boundary layer flow from the wall surfaces. To change the direction of wind in clockwise direction, the model is rotated in anticlockwise direction with the same flow parameters and boundary conditions.

8. Convergence of the solution

Convergence of the solution is judged by monitoring the solution variables. Monitor points of mass and momentum and the RMS of dissipation of kinetic energy (ϵ) and turbulent kinetic energy (k) reached at steady state condition during the simulation. The residual

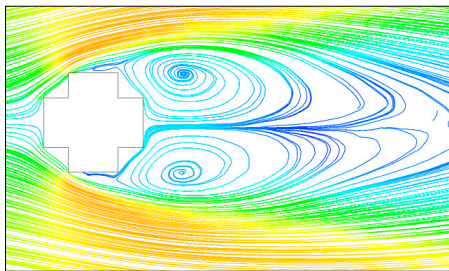
RMS error values was achieved between 10^{-4} to 10^{-5} for the momentum in three directions and up to 10^{-6} for mass and, the domain imbalances were found to be less than 0.001% for the momentum in three directions and zero for total mass.

7. Result and discussion

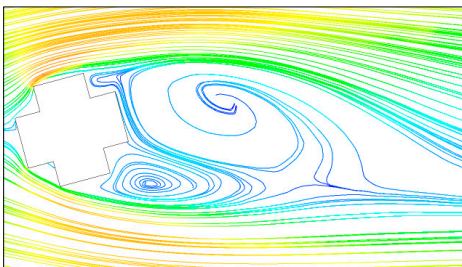
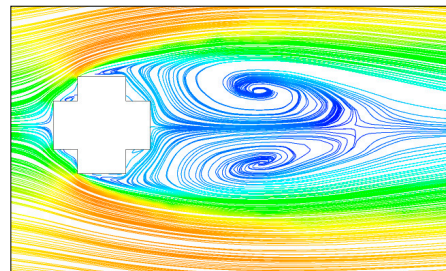
7.1. Flow Characteristics

7.1.1. Streamlines on Horizontal Planes

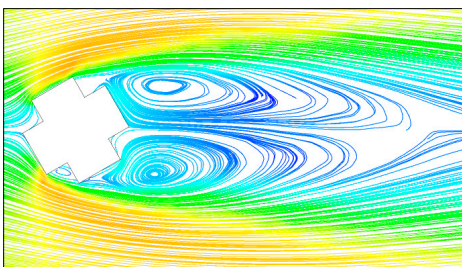
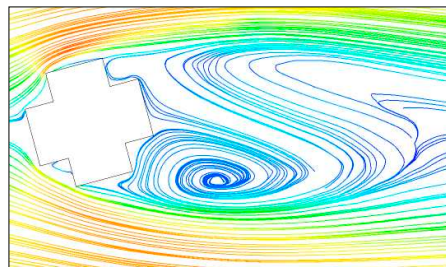
Separation of streamlines takes place before the flow hits the wind ward face. After hitting the leading edges, where velocity is maximum, recirculation zones are created all-round the building façade and roof. The flow reattaches after the wake region. In this region flow recirculation with high turbulence forming two distinct vortices is developed. Due to change in wind angles the pattern of formation of these vortices are different. Small vortex and recirculation of flow is created in the re-entrant corners specially in the high turbulence zones. Eddies created due to these vortices develop suction on the surfaces of the model. Flow streamlines at $1/3^{\text{rd}}$ and $2/3^{\text{rd}}$ of the model height for different wind angle are shown in figure 6 (a) to 6 (g).



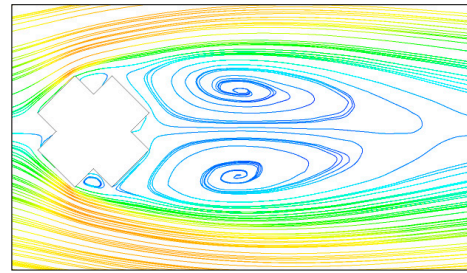
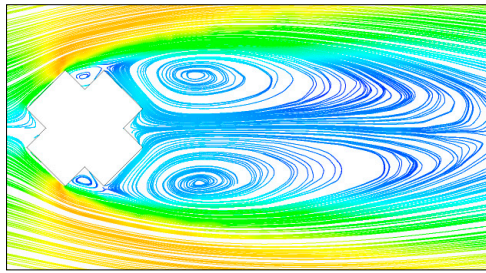
(a): Streamline Pattern at $1/3^{\text{rd}}$ and $2/3^{\text{rd}}$ height of model at 0° Wind Angle Respectively



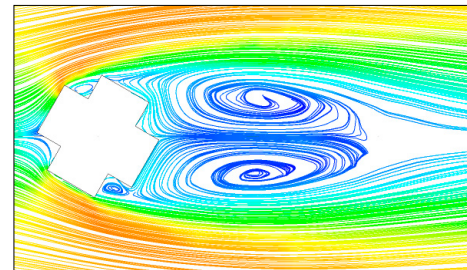
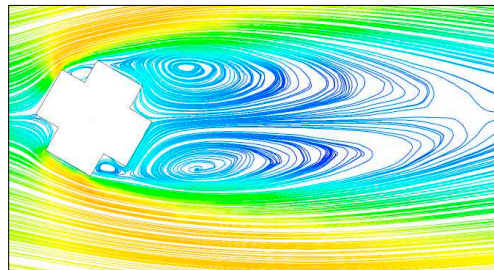
(b): Streamline Pattern at $1/3^{\text{rd}}$ and $2/3^{\text{rd}}$ height of model at 15° Wind Angle Respectively



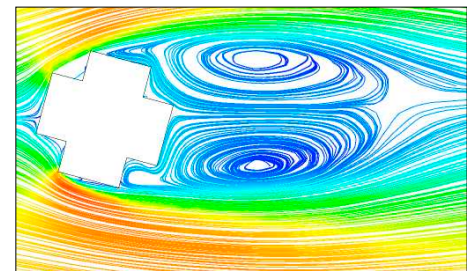
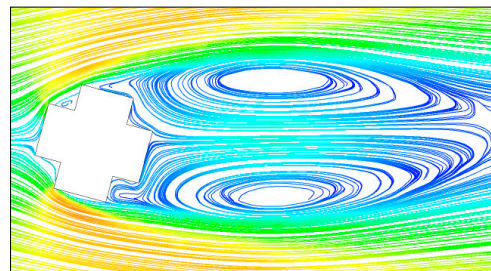
(c): Streamline Pattern at $1/3^{\text{rd}}$ and $2/3^{\text{rd}}$ height of model at 30° Wind Angle Respectively



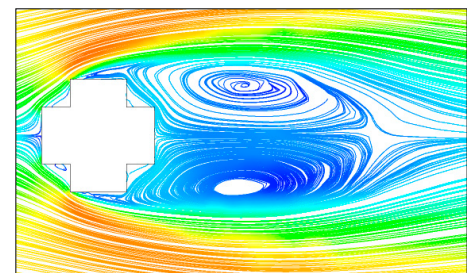
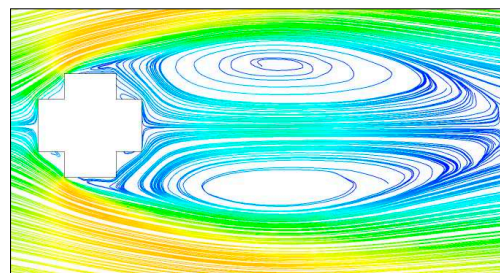
(d): Streamline Pattern at 1/3rd and 2/3rd height of model at 45° Wind Angle Respectively



(e): Streamline Pattern at 1/3rd and 2/3rd height of model at 60° Wind Angle Respectively



(f): Streamline Pattern at 1/3rd and 2/3rd height of model at 75° Wind Angle Respectively

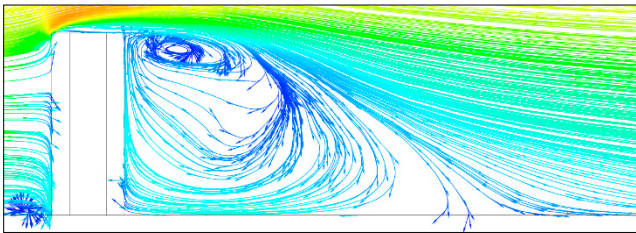


(g): Streamline Pattern at 1/3rd and 2/3rd height of model at 90° Wind Angle Respectively

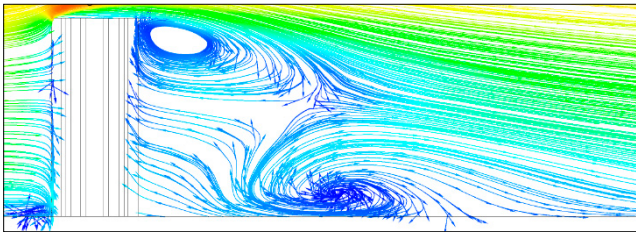
Figure 6. Streamline Pattern at 1/3rd and 2/3rd height of model at different Wind Incidence Angle.

7.1.2. Streamlines on Central Vertical Plane

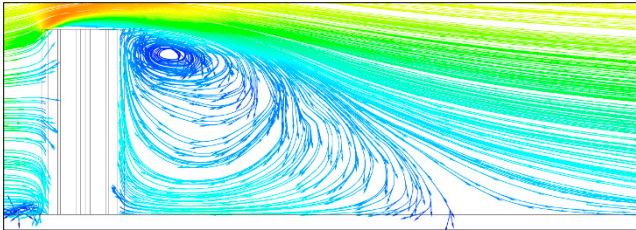
Figure 7a–g show streamline along the central vertical plane at varied wind angles of attack. The pattern of downwash zone, upwash zone and stagnation zone can be visualized from these. The upwind ground level vortex, shear layer at the roof and the pattern of vertical and horizontal recirculation of wind in the wake are clearly seen. It is observed that for 15° wind angle, the recirculation in the wake is prominent at two heights. At 45° wind angle, the shear layer formed at the roof is more protruding.



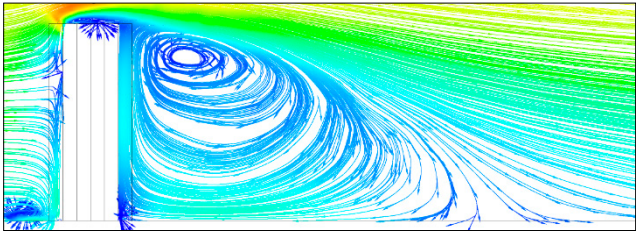
(a): Streamline Along Central Vertical Plane at 0° Wind Angle



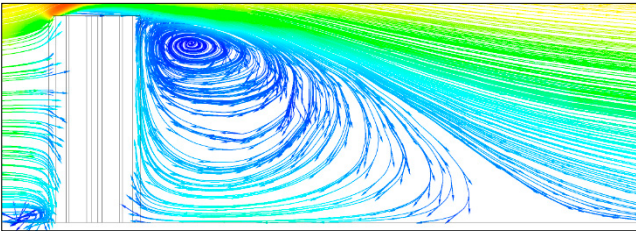
(b): Streamline Along Central Vertical Plane at 15° Wind Angle



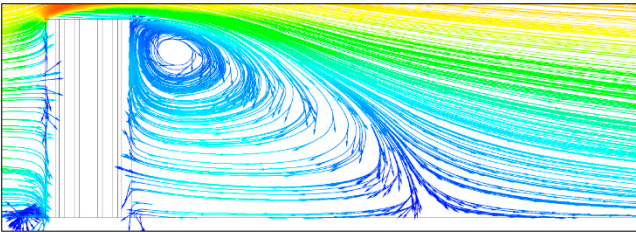
(c): Streamline Along Central Vertical Plane at 30° Wind Angle



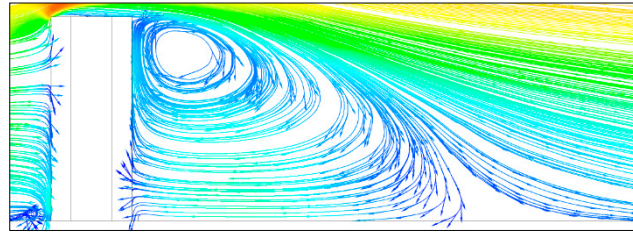
(d): Streamline Along Central Vertical Plane at 45° Wind Angle



(e): Streamline Along Central Vertical Plane at 60° Wind Angle



(f): Streamline Along Central Vertical Plane at 75° Wind Angle

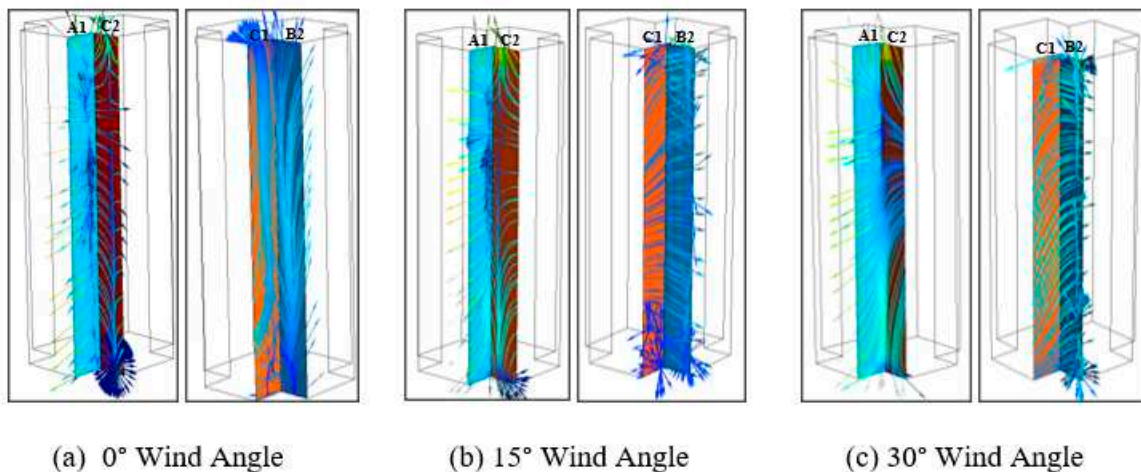


(g): Streamline Along Central Vertical Plane at 90° Wind Angle

Figure 7. Streamline Along Central Vertical Plane at different Wind incidence Angle.

7.1.3. Streamlines on Re-entrant Corner Faces

Owing to the model symmetry about both axes, study on corner faces A1-C2 and B2-C1 for extended angle of wind attack from 0° to 90° @ 15° are sufficient to understand the effect of wind incident angles on these faces. Streamlines on these faces have been shown in Figure 8a–g. At 0° wind angle, after impinging on the near edge of face C2, wind is striking at the outer edge of face A1, which is the leading edge. Face A1 is facing the wind directly too. It then reflects the wind on the side face C2. A downwash from face C2 creates a small vortex at the bottom of face C2. Back wash on both the faces B2 & C1 are observed. The streamline from face B2 is reflecting on face C1 and flow is predominantly escaping from the roof top of face C1. At 15° wind angle, the flow is separating from the leading edge of face A1. The stagnation of flow along the height is taking place on face A1 nearer to the corner than that at 0° wind angle. A frail vortex than that created at 0° wind angle is seen at the bottom. The backwash from the wake is creating a recirculation cavity after striking face C1. At 30° wind incidence angle, flow separation is taking place from the leading edge of face C2 and reflecting on face A1 before the separation takes place at the outer edge of face A1. The stagnation concentration is seen at the middle height. No ground level vortex is seen. In the corner of face B2 & C1, cavity recirculation is more prominent than that seen at 15° wind angle with a small vortex at the bottom of face B2. At 45° wind angle, the flow stagnation is at the corner of faces A1 & C2. The upwash and downwash zone are more prominent with almost no stagnation zone. No upwind vortex at ground level is created. At the corner of face B2 & C1, the downwash from the wake is striking both the faces. At 60° wind angle, the flow after striking the near end of face A1 is revolving into the corner and leaving from the outer edge of face C2. In the corner of faces B2 and C1, the flow is creating a concentration of upwash near the lower part of face C1. Circulation cavity is also seen in this re-entrant corner. At 75° wind angle, the wind is impinging on face C2 and reflecting to face A1, creating a small vortex at the bottom of face A1. At the corner of faces B2 & C1, wind is striking on face C1 and reflecting to face B2 creating a small vortex at the bottom of face B2. At 90° wind angle both the corners are on the windward side. The stagnation of wind on faces C1 & C2 takes place reflecting to faces B2 and A1 respectively, separating from the respective leading edges of their faces.



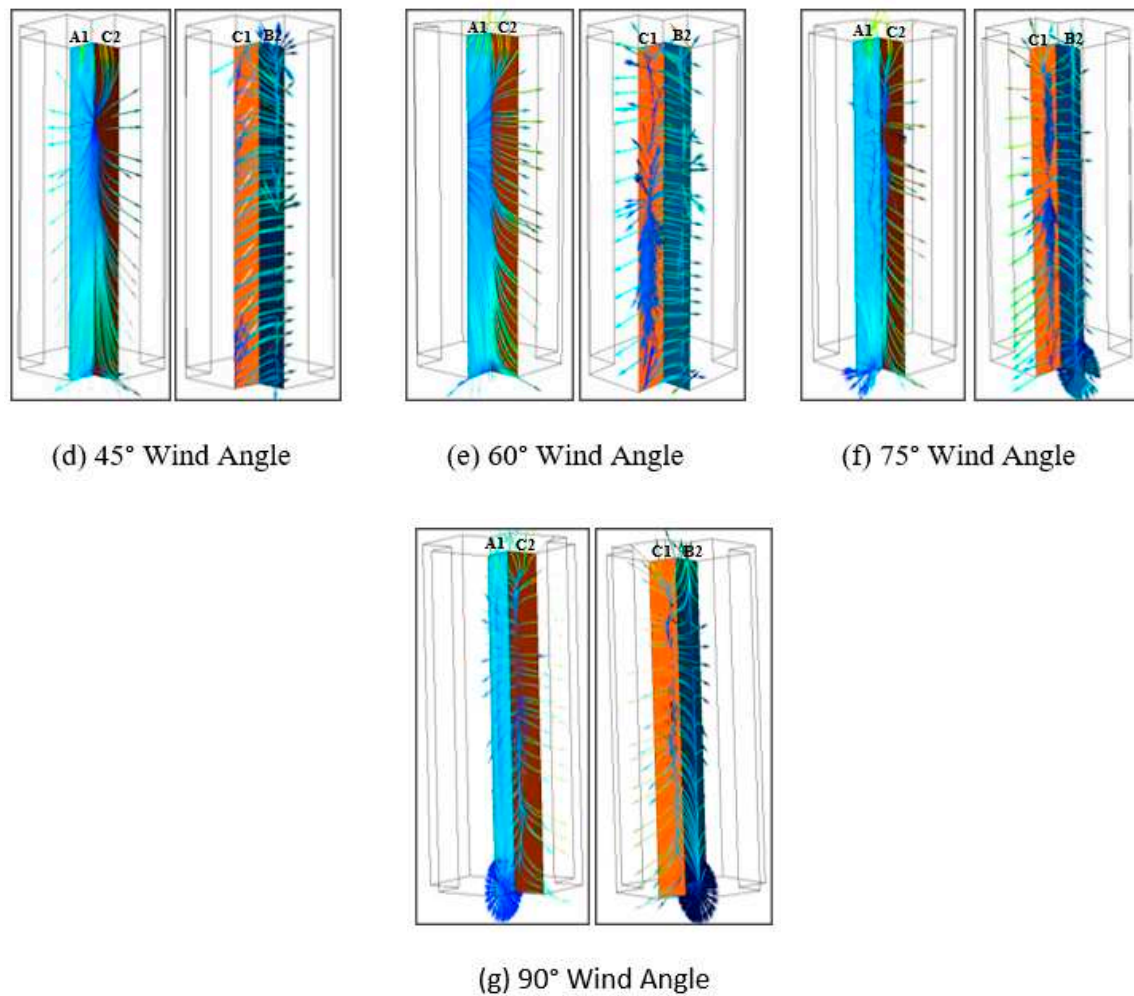
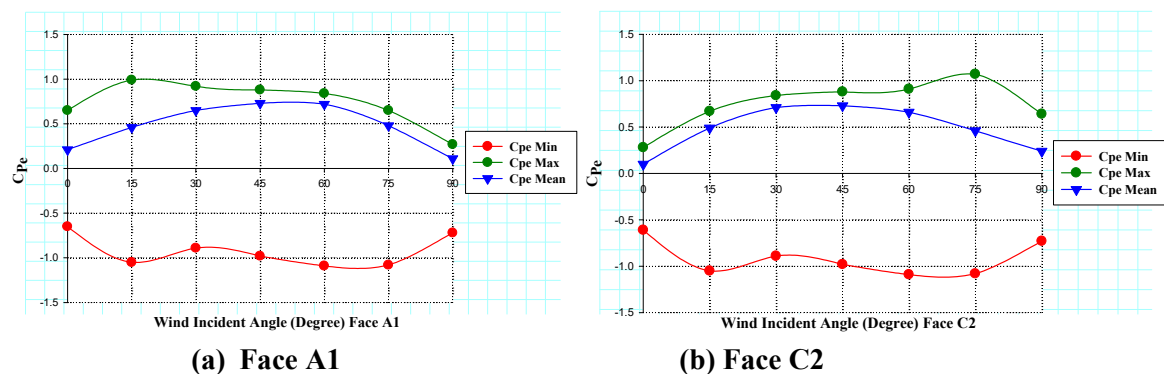


Figure 8. Streamlines on Re-entrant Corner Faces.

7.2. Pressure/ Pressure Coefficient on Re-entrant Faces

7.2.1. Minimum, Maximum and Mean C_{pe}

The variation of minimum, maximum and area average value of C_{pe} on different re-entrant corner faces (A1, C2, B2 & C1) are shown in Figure 9a–d for 0° to 90° @ 15° wind angle. For faces A1 & C2 it is seen that the minimum value of C_{pe} for all the wind angles are almost same. The maximum value of C_{pe} on these faces varying with wind angles. The maximum C_{pe} is at 45° wind angle. For the faces B2 & C1, the minimum C_{pe} on face B2 is at 45° and on face C1 is at 90° wind angles respectively. The maximum C_{pe} on these faces are at 90° wind incident angle for the respective faces. The maximum face averaged values are also found to be at 90° for the respective faces.



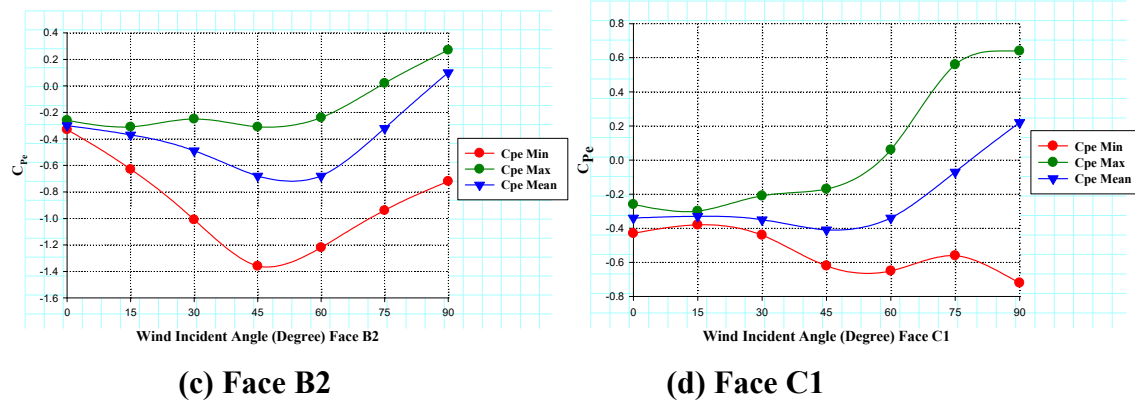
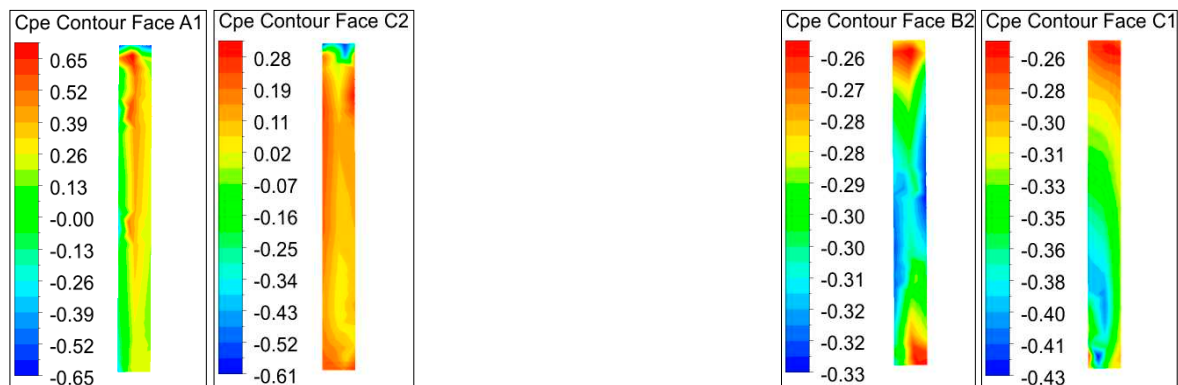


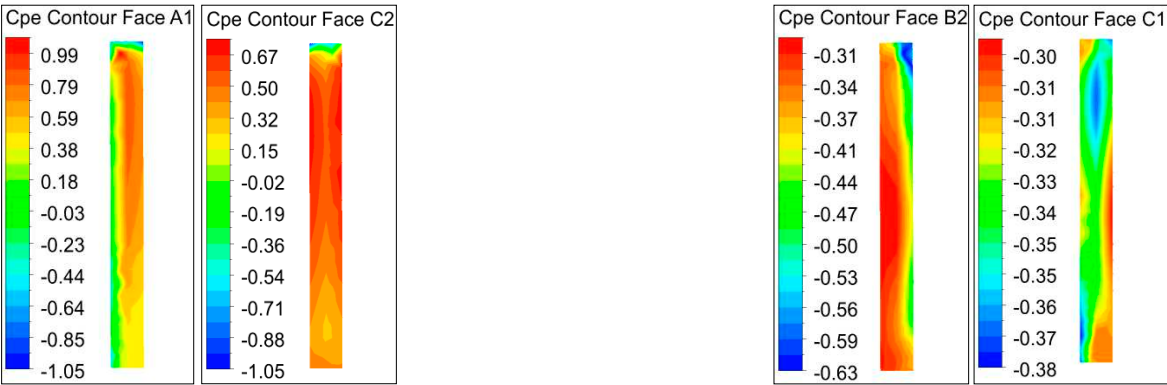
Figure 9. Variation of C_{pe} on Re-entrant Faces with Wind Angle.

7.2.2. C_{pe} Contours

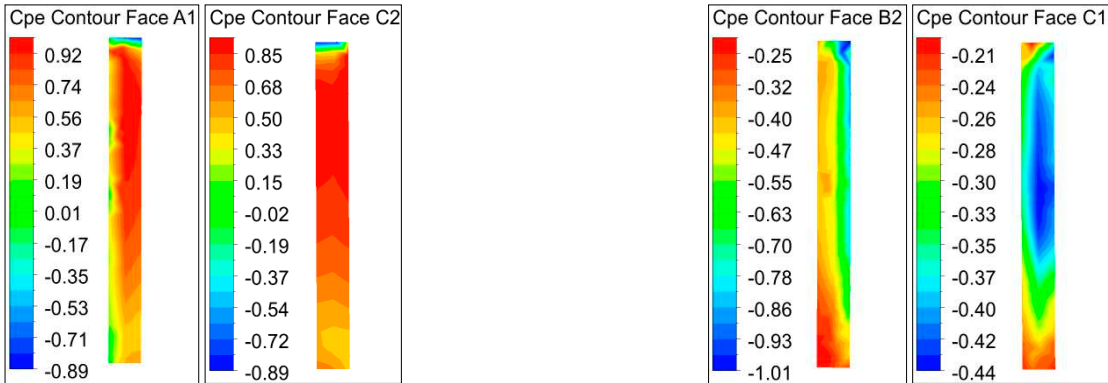
The C_{pe} contours on these faces are shown in Figure 10a–g. At 0° wind incident angle, face A1 being on the upwind direction is predominantly facing positive pressure with negative pressure at the top corners. The positive pressure is predominant towards the outer edge of face A1 with a concentration of high positive pressure forming near the top. Unlike the case of rectangular model where side faces are subjected to negative pressure, face C2 is facing positive pressure due to interference effect from face A1. The pressure is concentrated towards re-entrant corner. Negative pressure is seen in a small zone near the top. From 0° to 30° wind angle, C_{pe} is varying on these faces on the same outline as discussed above. At 45° wind angle, both the faces facing the direct wind are encountered with same pressure pattern on their faces with a maximum C_{pe} values on the faces. From 60° to 90° the pressure pattern on these faces is interchanged with each other as that from 30° to 0° wind angle. On the downwind side, face B2 is under negative pressure of almost uniform nature. Concentration of maximum negative pressure is observed at the bottom, near outer edge of face B2 and also at the top, near the re-entrant corner. Pressure on face C1 is concentrated towards the top at re-entrant corner. Unlike the re-entrant corner faces A1 & C2 which are facing positive pressure from 0° to 90° wind angle, being on the windward side, the pressure on faces B2 & C1 changes as the surfaces are facing the wake region, then to side faces and then to windward side due to change in wind direction. Effect of local eddies in the form of concentration of colors are observed on the faces due to high turbulence and micro level vortices.



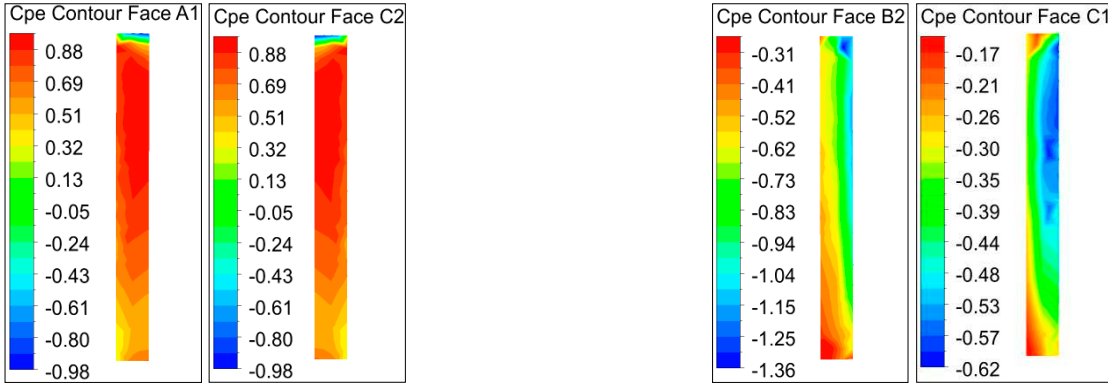
(a): C_{pe} Counter for 0° Wind Angle



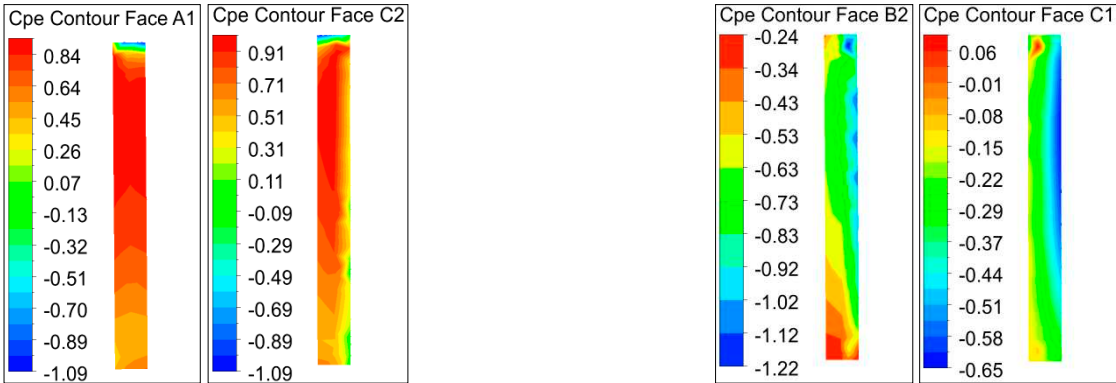
(b): C_{pe} Counter for 15° Wind Angle



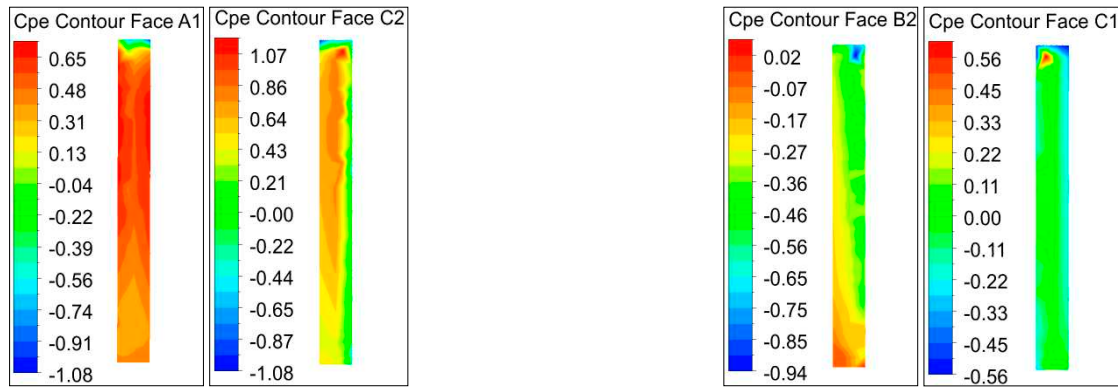
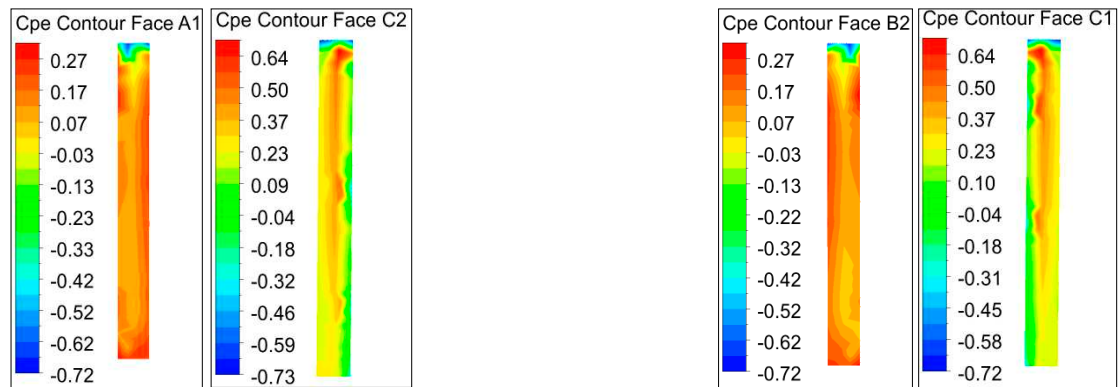
(c): C_{pe} Counter for 30° Wind Angle



(d): C_{pe} Counter for 45° Wind Angle

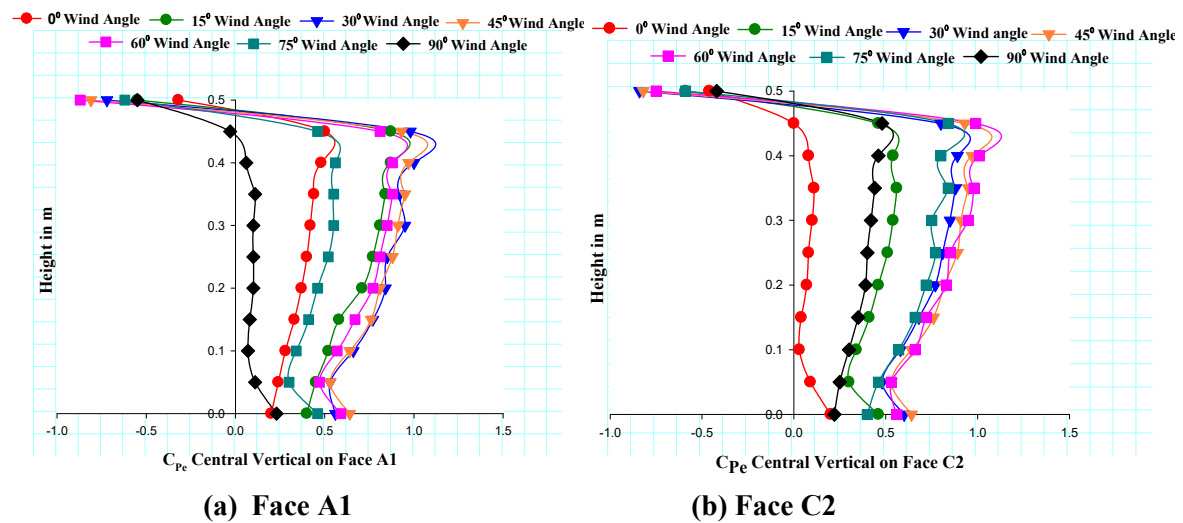


(e): C_{pe} Counter for 60° Wind Angle

(f): C_{pe} Counter for 75° Wind Angle(g): C_{pe} Counter for 90° Wind AngleFigure 10. C_{pe} Counter for different Wind Incidence Angle.

7.2.3. Central Vertical C_{pe} on Faces

Figure 11a–d shows C_{pe} on central vertical line on faces A1, C2, B2 & C1. Positive pressure exists on the face exposed to direct wind. It can be clearly observed that faces A1 & C2 are experiencing positive pressure for all the wind angles from 0° to 90°. On Face A1, very minute variation of C_{pe} values are observed for wind angles 15°, 30°, 45° & 60°. But, on face C2 minute variation are seen at 30°, 45°, 60° & 75° wind angles. On faces B1 and C2, the central vertical pressure is mostly negative except at wind angle 90°. The same observation is seen on face C1 with the exception that at wind angle 75°, it is almost zero throughout the height.



(a) Face A1

(b) Face C2

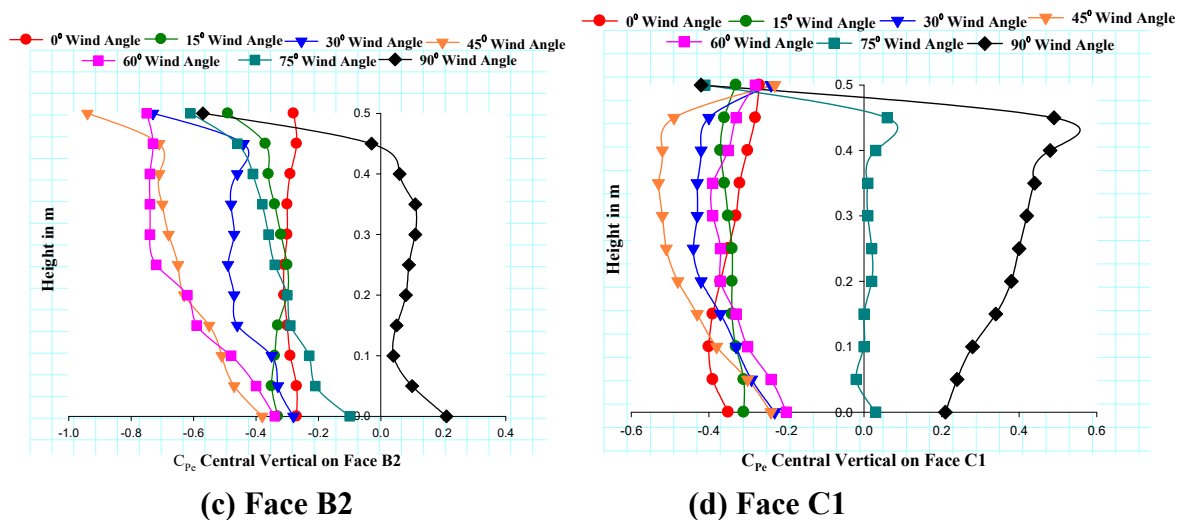


Figure 11. C_{pe} Variation along Central Vertical Line for Wind Angles.

8. Conclusion

The current research study is valuable to investigate the effect of wind on plus-shaped buildings, emphasizing the significance of different wind incidence angles. The present study is performed on re-entrant corner of tall building using numerical technique ANSYS CFX and few of the important outcomes from the study are as follow:

- The study observed substantial influence of wind incidence angles on the corner faces of plus plan-shaped buildings in terms of the variations in pressure on these for different wind incidence angles.
- The height of the building and the relative length dimensions of the wing faces are crucial factors affecting the pressure distribution on these faces. These factors are particularly important for designing cladding units necessitating consideration by design engineers.
- The simulation results demonstrate good agreement, especially for wind directions orthogonal to the building's faces, some differences are noted for other wind angles due to the complex, anisotropic, unsteady three-dimensional flow behavior of wind.
- The influence of streamlines in the bottom portion of the structure is relatively minimal while the upper portion exhibits the presence of robust vortices, particularly noticeable within wind angles varies from 0 to 30 degrees.
- The vortices remain relatively consistent in size and intensity for both the top and bottom portion in the case of 45-degree wind incidence angle.
- For tall buildings with re-entrant corners, the research revealed a notable stagnation zone at a 30-degree wind incidence angle, located at the mid-height of the model. Flow separation was observed originating from the leading edge under these conditions
- A circulation cavity was evident on the re-entrant corner of the building when wind is striking the building at 75-degree wind. It was observed that the size of vortices on the re-entrant corner remains consistent for wind angles of 0 and 90 degrees.
- The data observed may be utilized by architects for ventilation planning and structural designers for accurate wind load analysis, contributing to more effective and informed engineering calculations.

Author Contributions: Conceptualization, A.K., and R.K.M.; Methodology, A.K., R.K.M. and R.R.; Software, A.K., R.K.M. and R.R.; Validation, R.R.; Formal analysis, A.K. and R.K.M.; Resources, M.I.K and J.M.K.; Writing – original draft, A.K. and R.K.M.; Writing – review & editing, R.R., R.K.M., M.I.K. and J.M.K; Supervision, R.R. All authors have read and agreed to the published version of the manuscript.

Funding: The authors extend their appreciation to Researcher Supporting Project number (RSPD2023R692), King Saud University, Riyadh, Kingdom of Saudi Arabia.

Institutional Review Board Statement: Not applicable.

Informed Consent Statement: Not applicable.

Data Availability Statement: Not applicable.

Acknowledgments: The authors extend their appreciation to Researcher Supporting Project number (RSPD2023R692), King Saud University, Riyadh, Kingdom of Saudi Arabia.

Conflicts of Interest: The authors declare no conflict of interest.

References

1. A. Rukhaiyar, B. Jayant, K. Dahiya, R. K. Meena, and R. Raj, "CFD simulations for evaluating the wind effects on high-rise buildings having varying cross-sectional shape," *Journal of Structural Fire Engineering*, vol. 14, no. 3, pp. 285–300, 2023, doi: 10.1108/JSFE-04-2022-0016.
2. R. K. Meena, R. Raj, and S. Anbukumar, "Effect of wind load on irregular shape tall buildings having different corner configuration," *Sadhana - Academy Proceedings in Engineering Sciences*, vol. 47, no. 3, 2022, doi: 10.1007/s12046-022-01895-2.
3. R. K. Meena, R. Raj, and S. Anbukumar, "Wind Excited Action around Tall Building Having Different Corner Configurations," *Advances in Civil Engineering*, vol. 2022, no. 2022, 2022, doi: <https://doi.org/10.1155/2022/1529416>.
4. IS: 875 (2015), *Indian Standard design loads (other than earthquake) for buildings and structures-code of practice, part 3(wind loads)*. 2015.
5. Hong Kong Building Department, GB 50009-2001, ASCE: 7-16(2017), AS/NZS:1170.2(2011), and IS: 875 (2015), *Structural Design Actions - Part 2: Wind actions. Standards Australia/Standards New Zealand, Sydney*, no. 7 98. 2011. doi: 10.1061/9780872629042.
6. ASCE: 7-16(2017), *Minimum Design Loads and Associated Criteria for Buildings and Other Structures. Structural Engineering Institute of the American Society of Civil Engineering, Reston*, no. 7 98. 2017. doi: 10.1061/9780872629042.
7. ASCE: 49-12(2012), *Wind Tunnel Testing for Buildings and Other Structures. Structural Engineering Institute of the American Society of Civil Engineering, Reston. American Society of Civil Engineers 1801 Alexander Bell Drive Reston, Virginia 20191* www.asce.org/pubs, 2012.
8. AS/NZS, "AS-NZS 1170-2 (2011) (English): Structural design actions - Part 2: Wind actions [By Authority of New Zealand Structure Verification Method B1 / VM1]," vol. 2, 2011.
9. ETHIOPIAN STANDARD, *ES ISO 4354 (2012) (English): Wind actions on structures*, vol. 2012. 2012. [Online]. Available: http://scholar.google.com/scholar?start=10&q=asi+interface&hl=es&as_sdt=0,5#6
10. M. G. Gomes, A. Moret Rodrigues, and P. Mendes, "Experimental and numerical study of wind pressures on irregular-plan shapes," *Journal of Wind Engineering and Industrial Aerodynamics*, vol. 93, no. 10, pp. 741–756, 2005, doi: 10.1016/j.jweia.2005.08.008.
11. P. Mendis, T. Ngo, N. Haritos, A. Hira, B. Samali, and J. Cheung, "Wind Loading on Tall Buildings," *EJSE: loading on structures*, vol. 7, pp. 51–54, 2007.
12. J. Y. Fu, Q. S. Li, J. R. Wu, Y. Q. Xiao, and L. L. Song, "Field measurements of boundary layer wind characteristics and wind-induced responses of super-tall buildings," *Journal of Wind Engineering and Industrial Aerodynamics*, vol. 96, no. 8–9, pp. 1332–1358, Aug. 2008, doi: 10.1016/j.jweia.2008.03.004.
13. Tanaka H, Tamura Y, Ohtake K, Nakai M, Kim YC, and Bandi E K, "Experimental Investigation of Aerodynamic Forces and Wind Pressure Acting on Tall Buildings with Various Unconventional Configuration," *Journal of Wind Engineering and Industrial Aerodynamics*, vol. 107–108, pp. 179–191, 2013.
14. J. A. Amin and A. K. Ahuja, "Effects of Side Ratio on Wind-Induced Pressure Distribution on Rectangular Buildings," *Journal of Structures*, vol. 2013, pp. 1–12, Aug. 2013, doi: 10.1155/2013/176739.
15. B. Bhattacharyya, Dalui S.K, and Ahuja A.K, "Wind Induced Pressure on 'E' Plan Shaped Tall Buildings," *Jordan Journal of Civil Engineering*, vol. 8, no. 2, pp. 120–134, Apr. 2014, [Online]. Available: <https://www.researchgate.net/publication/264548132>
16. J. Yi and Q. S. Li, "Wind tunnel and full-scale study of wind effects on a super-tall building," *J Fluids Struct*, vol. 58, pp. 236–253, Oct. 2015, doi: 10.1016/j.jfluidstruct.2015.08.005.
17. A. Mukherjee and A. K. Bairagi, "Wind Pressure and Velocity Pattern Around 'N' Plan Shape Tall Building-A Case Study," in *Asian J. Civil Eng*, 2017, pp. 1241–1258.
18. M. Mallick, A. Mohanta, A. Kumar, and V. Raj, "Modelling of Wind Pressure Coefficients on C-Shaped Building Models," *Modelling and Simulation in Engineering*, vol. 2018, pp. 1–13, 2018, doi: 10.1155/2018/6524945.
19. B. S. Chauhan and A. K. Ahuja, "Response of Tall Building Subjected to Wind Loads Under Interference Condition," *International Journal of Civil Engineering and Technology (IJCIET)*, vol. 11, no. 2, pp. 156–163, 2020, [Online]. Available: <http://www.iaeme.com/ijcieta/issues.asp?JType=IJCIET&VType=11&IType=2http://www.iaeme.com/IJCIE T/issues.asp?JType=IJCIET&VType=11&IType=2>

20. P. K. Goyal, S. Kumari, S. Singh, R. K. Saroj, R. K. Meena, and R. Raj, "Numerical Study of Wind Loads on Y Plan-Shaped Tall Building Using CFD," *Civil Engineering Journal*, vol. 8, no. 02, pp. 263–277, 2022.
21. P. Sanyal and S. K. Dalui, "Effects of side ratio for 'Y' plan shaped tall building under wind load," *Build Simul*, vol. 14, no. 4, pp. 1221–1236, Aug. 2021, doi: 10.1007/s12273-020-0731-1.
22. R. Raj and A. Kumar Ahuja, "Wind Loads on Cross Shape Tall Buildings," *Journal of Academia and Industrial Research*, vol. 2, no. 2, pp. 111–113, 2013.
23. S. Chakraborty, S. K. Dalui, and A. K. Ahuja, "Experimental Investigation of Surface Pressure on '+' Plan Shape Tall Building," *Jordan Journal of Civil Engineering*, vol. 8, no. 3, pp. 251–261, 2014.
24. ANSYS Inc, *ANSYS CFX-Solver Theory Guide*. 2009. [Online]. Available: <http://www.ansys.com>
25. J. Franke *et al.*, "Impact of wind and storm on city life and built environment," *Recommendation on the use of CFD in Wind Engineering. In: COST action C14*, vol. Version 1.0, pp. 1–12, 2004.
26. Revuz J, Hargeaves D. M, and Owen J.S., "On the Domain Size for the Steady State CFD Modeling of a Tall Building," *Wind Structure*, vol. 15, no. 4, pp. 313–329, 2012.

Disclaimer/Publisher's Note: The statements, opinions and data contained in all publications are solely those of the individual author(s) and contributor(s) and not of MDPI and/or the editor(s). MDPI and/or the editor(s) disclaim responsibility for any injury to people or property resulting from any ideas, methods, instructions or products referred to in the content.